Temperature-Induced Micelle Formation of a Diblock Copolymer of Styrene and *tert*-Butylstyrene in *N,N*-Dimethylacetamide

Zukang Zhou,† Benjamin Chu,*,†,‡ and Dennis G. Peiffer§

Chemistry Department, State University of New York at Stony Brook, Long Island, New York 11794-3400, Department of Materials Science and Engineering, State University of New York at Stony Brook, Long Island, New York 11794-2275, and Corporate Research Science Laboratory, Exxon Research and Engineering Company, Clinton Township, Annandale, New Jersey 08801

Received October 23, 1992; Revised Manuscript Received December 29, 1992

ABSTRACT: Static and dynamic light-scattering studies are presented on the temperature-induced associating behavior of a polystyrene–poly(*tert*-butylstyrene) block copolymer in a selective solvent *N,N*-dimethylacetamide. On cooling from 65 °C down to room temperature, three temperature regions of unimer, transition, and micellar particles appeared sequentially. The molecular weight and the hydrodynamic radius of the polymeric micelles formed at 25 °C were found to be 1×10^7 g mol^{-1} and 50 nm, respectively, whereas those of unimers examined at 60 °C were 2×10^5 g mol^{-1} and 10 nm, respectively. In both cases, a narrow size distribution was observed. In the intermediate transition region, dynamic light-scattering measurements have clearly demonstrated a temperature- and concentration-dependent equilibrium between single polymer chains and polymer micelles. From the concentration dependence of the critical micelle temperature, the standard enthalpy of micellization was estimated to be −240 kJ mol^{-1}. A closed association model with the enthalpy factor as the driving force is discussed. On the basis of the mass action law model of micelle formation and the time-averaged scattered intensity results or the results of bimodal relaxation rate distributions in the transition region obtained by the CONTIN analysis, we were able, for the present system, to estimate the critical micelle concentration and related standard thermodynamic functions of micellization.

Introduction

In the past two decades block copolymer solutions have received considerable attention in the literature.[1-3] One of the major reasons is that in analogy to the widely used synthetic surfactants, block copolymers exhibiting amphiphilic nature can self-assemble into organized structures in various selective solvents, thereby creating useful microenvironments under controlled conditions for a number of specific purposes, such as controlled drug release. For some types of block copolymer, for example, copolymers of ethylene oxide and propylene oxide, the association into reverse micelles in organic medium as well as the formation of direct micelles in aqueous solution has been reported.[4-9] Recently, the micellar solutions of a triblock copolymer of styrene and hydrogenated butadiene in a selective solvent either for the end blocks or for the middle block were studied.[10]

In general, temperature is an important and useful factor in controlling a variety of physico–chemical processes of block copolymers in solution. In a previous article[6] we reported in detail the temperature-induced micellization behavior of a triblock copolymer Pluronic F68 (poly(oxyethylene)–poly(oxypropylene)–poly(oxyethylene)) in water. Three temperature regions were found, and they were unimer, transition, and micelle regions, existing at ambient, intermediate, and high temperatures, respectively. The mechanism behind can be ascribed to the considerable modification of the hydrophilic–hydrophobic characteristics of polymeric surfactant molecules by changing the temperature. Recent studies[11,12] on similar block copolymers further confirmed that the entropy factor is essentially responsible for the micellization process. Very recently, similar thermodynamic studies were reported on the micelle formation of polystyrene-*b*-poly(ethylene/propylene) in various selective solvents.[13,14]

We have chosen diblock copolymers of styrene and *tert*-butylstyrene as model systems to investigate their reversible aggregation behavior in both the solution and the bulk state. The advantages are (1) unlike the conventional block copolymers with accompanying composition heterogeneity, polystyrene-*b*-poly(*tert*-butylstyrene) (PS-*b*-P(*t*-BS)) samples with well-defined composition and controlled block length are available on a laboratory scale and are nearly monodisperse, (2) the two polymer components are similar to each other in their chemical structure, and (3) the properties can be modified by introducing some functional groups to meet the specific requirements. In this article, we report, as a part of our fundamental work, some static and dynamic light-scattering results on the temperature-induced associating behavior of a PS-*b*-P(*t*-BS) copolymer (molar ratio 1:1) in *N,N*-dimethylacetamide (DMA) which is a good solvent for the PS block but a nonsolvent at room temperature for the P(*t*-BS) part. In contrast to the PEO–PPO–PEO/water system, where an increase in temperature may cause remarkable micellization, dilute solutions of PS-*b*-P(*t*-BS) in DMA undergo micelle formation upon *reducing* the temperature. In the latter case, the enthalpy factor is the driving force for micellization, while the entropy contribution is responsible in the former case.

For the present model system the transition region observed is relatively sharp (only ~4–5 deg), and both the unimer and the micellar particles formed have narrow size distributions. Thus, on the basis of the knowledge on the equilibrium concentrations of unimers and of micelles in solution, which could be obtained by either using the CONTIN method[15] or analyzing the scattered intensity data, we were able to determine the critical micelle concentration and to estimate standard thermodynamic functions of the micelle formation.

Experimental

Materials. For our investigations we used the polystyrene-*b*-poly(*tert*-butylstyrene) sample which has a molecular weight of 1.85×10^5 g mol^{-1} and a polydispersity index of 1.10. PS-*b*-P(*t*-BS)

* To whom correspondence should be addressed.
† Chemistry Department.
‡ Department of Materials Science and Engineering.
§ Corporate Research Science Laboratory.

0024-9297/93/2226-1876$04.00/0

contains ~700 repeat units for each of the component blocks. The *N,N*-dimethylacetamide solvent was of HPLC grade, purchased from Aldrich Co., and was used without further treatment.

Copolymer solutions were prepared from dilutions of the same stock solution. The stock solution ($C \simeq 4$ mg mL^{-1}) was obtained by dissolving a known amount of copolymer in DMA under gentle agitation and then heating it at 60 °C for 6 h to ensure complete dissolution. At room temperature the stock solution was then centrifuged at 10 000 rpm (≃12 000*g*) for 1 h. To prepare solutions with the desired concentration, clarified stock solution and solvent were filtered separately in appropriate amounts through Millipore fluoropore membrane filters (0.2-μm pore size) into 17-mm-o.d. light-scattering cells. The solution cells were flame-sealed under vacuum and stored.

Light Scattering Measurements. We used a standard, laboratory-built light-scattering spectrometer[6] capable of both time-averaged scattered intensity and photon correlation measurements at different scattering angles. A Spectra-Physics Model 165 argon ion laser operated at 488 nm was used as the light source. A high-quality beam splitter was installed on the main beam path to function as an attenuator, thus making measurements of greatly differing scattering signals (e.g. by a factor of 10^3) feasible and rather convenient. In our case, an additional advantage was to provide the same light source for a second light-scattering setup. The sample cell was held in a brass thermostat block filled with refractive index matching fluid (silicone oil), and the temperature was controlled to within ±0.02 °C. In the present study the temperature range covered was 25–65 °C. Static light-scattering measurements were performed at angles between 25 and 140°. Photon correlation measurements were carried out in the self-beating mode by using Brookhaven BI 2030AT digital correlators consisting of 64 or 128 channels. The cumulants[16] and CONTIN methods were used for data analysis to extract information on the average hydrodynamic size or the distribution of characteristic relaxation rates, respectively. In most cases, dynamic light-scattering experiments were made at scattering angle $\theta = 45°$.

Results and Discussion

1. Critical Micelle Temperature and Three Temperature Regions. The intensity of scattered light is largely dependent on the volume of the scatterer. Therefore light scattering is a powerful technique for the purpose of detecting the onset of micellization in polymeric micellar solutions. In general, the micelle formation can be initiated either by an increase in concentration via the critical micelle concentration (cmc) or by changing the temperature via the critical micelle temperature (cmt). Experimentally, the micellization process can be studied by defining the cmt through the temperature dependence of either the integrated scattered light intensity or the hydrodynamic size of the particles, provided that the transition is reasonably sharp. Similarly, an examination of the concentration dependence gives the cmc value. Figure 1 shows the scattered intensity results measured at a scattering angle of 45° for the copolymer solution at four differing concentrations of 0.51, 1.02, 1.94, and 3.77 mg mL^{-1}, respectively. As seen from Figure 1, below a certain temperature value which is characteristic of the solution concentration concerned, a distinct increase in intensity occurred over a relatively narrow temperature interval. This transition point which can be defined as the critical micelle temperature exists on all the intensity–temperature curves. The meaning is that above the cmt, essentially constant but very low scattered intensities were detected. In this region the weight-average molecular weight determined by extrapolating the intensity data to infinite dilution, as will be discussed later, is 2.0×10^5 g mol^{-1}, in good agreement with the molecular weight value of 1.85×10^5 g mol^{-1} for single copolymer chains. Obviously, only unimers are practically present above the critical micelle temperature. When the temperature

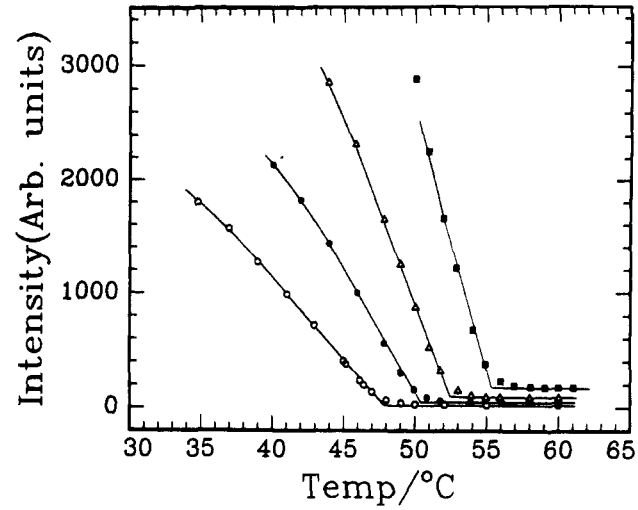

Figure 1. Plots of the excess scattered intensity (measured at $\theta = 45°$, in arbitrary units) versus temperature for the PS-*b*-P(*t*-BS) copolymer in *N,N*-dimethylacetamide: (open circles) $C = 0.51$ mg mL^{-1}; (filled circles) 1.02 mg mL^{-1}; (open triangles) 1.94 mg mL^{-1}; (filled squares) 3.77 mg mL^{-1}. The intersections of two straight lines define the critical micelle temperatures. They are 47.9, 50.4, 52.4, and 55.3 °C, respectively.

becomes lower than the cmt, micelle formation becomes increasingly important. Correspondingly, the light-scattering intensity increases appreciably. For block copolymer solutions, as we discussed elsewhere,[6] usually a certain transition region rather than a sharp inflection on the temperature curve can be expected. Nevertheless, from the intersection of two straight-line portions, as shown in Figure 1, we could estimate the cmt value. We thus obtained cmt values of 47.9, 50.4, 52.4, and 55.3 °C for the above four concentrations in ascending order. Alternatively, we can consider, to a first approximation, the concentration which is related to each experimental curve in Figure 1 as the critical micelle concentration at the corresponding cmt. Accordingly, for the PS-*b*-P(*t*-BS)/DMA system studied, the cmt shifts to a higher value with increasing concentration and the cmc shifts to a lower concentration with decreasing temperature. In essence, the micellization reflects the tendency of keeping apart from the medium and self-assembling into ordered structures. In this connection, the above temperature-dependent association behavior can be understood on the basis of the observation that at room temperature the poly(*tert*-butylstyrene) homopolymer itself ($M = 2.07 \times 10^5$ g mol^{-1}) does not dissolve in DMA but becomes soluble at elevated temperatures (e.g. 60 °C).

The above conclusion about the cmt is further supported by the dynamic light-scattering results. Two curves of R_h(apparent) vs temperature, obtained for the 0.51 and 3.04 mg mL^{-1} solutions by using the cumulants method for data analysis, are shown in Figure 2. Figure 2 clearly demonstrates the existence of three temperature regions, namely unimer, transition, and micelle regions. They appeared in sequence with decreasing temperature. Firstly, in the high-temperature region (above cmt) relatively small ($R_h \simeq 10$ nm), but constant size (independent of temperature) and nearly monodisperse (variance $\mu_2/\bar{\Gamma}^2 \leq 0.02$), particles were detected, which convincingly supports the concept that only single polymer chains are present above the critical micelle temperature. Secondly, in the transition region consisting of a temperature interval of about 5 deg below the cmt, two distinct features were observed: an abrupt increase of the average particle size and a marked increase in the variance, both indicating that mixtures of unimer and micelle in equilibrium were

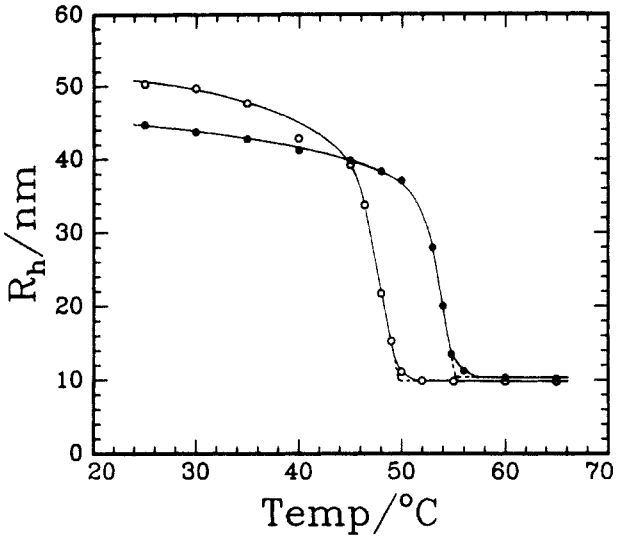

Figure 2. Plots of the apparent hydrodynamic radius (obtained at $\theta = 45°$) as a function of temperature for the PS-*b*-P(*t*-BS) copolymer in DMA. Open circles denote $C = 0.51$ mg mL^{-1}, and filled circles denote $C = 3.04$ mg mL^{-1}. The intersections of two straight lines define the critical micelle temperatures. They are 49.8 and 55.3 °C.

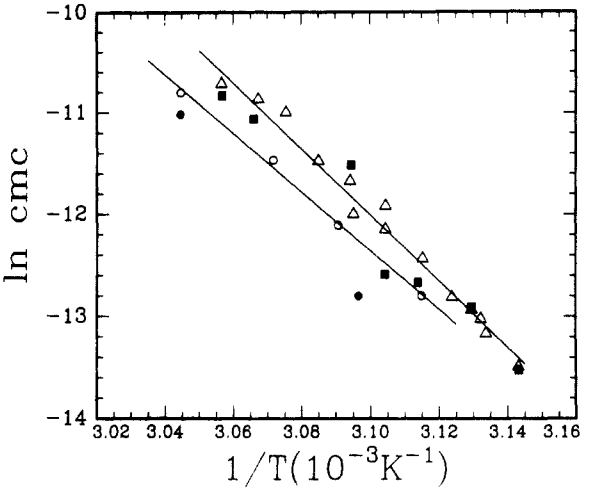

Figure 3. Plots of the logarithmic critical micelle concentration against the reciprocal of the absolute temperature. For the bottom line, open circles denote the data obtained from Figure 1; filled circles are from Figure 2. For the top line, filled squares denote the results obtained from the CONTIN analysis; open triangles are by the intensity analysis. The least squares fit yields ΔH^0 values of −240 ± 10 and −270 ± 10 kJ mol^{-1}, respectively.

present in this region. On the basis of the relaxation rate distributions derived from the CONTIN analysis, a more detailed discussion on the equilibrium will be given later. As shown in Figure 2, from the dynamic light-scattering data the cmt values were found to be 49.8 and 55.3 °C for the 0.51 and 3.04 mg mL^{-1} polymer solutions, respectively. These values are 1–2 deg higher than those obtained from the intensity measurements (Figure 1). Such variation can be understood if we consider the difference in the sensitivity to the onset of micellization between different methods. Finally, when temperature was further decreased, the micelle region was reached where only large particles ($R_h \simeq 40$–50 nm) with small variance ($\mu_2/\bar{\Gamma}^2 \simeq 0.02$) were found. This is consistent with the weight-average micellar molecular weight value of $\sim 1 \times 10^7$ g mol^{-1} at 25 °C, as will be given later. The intermicellar interactions may account for the variation of the apparent R_h value for the two concentrations given in Figure 2.

2. Thermodynamic Functions of Micellization. For a closed association mechanism with relatively large association number and narrow distribution, the standard free energy and standard enthalpy of micelle formation ($\Delta G°$ and $\Delta H°$, per mole of the solute in the micelle) are related to the critical micelle concentration and its temperature dependence in the form[17]

$$\Delta G° = RT \ln(\text{cmc}) \quad (1)$$

$$\Delta H° = R[\text{d} \ln(\text{cmc})/\text{d}(1/T)] \quad (2)$$

where the cmc is in molar concentration; the two standard states are the polymer molecules and micelles in ideally dilute solution at unity molarity. Equation 2 can be integrated to yield

$$\ln(\text{cmc}) \simeq \Delta H°/RT + \text{constant} \quad (3)$$

provided that $\Delta H°$ is approximately a constant in the temperature interval involved. In our case, as noted above, the values of cmt and C can be used instead of T and cmc. On the basis of eq 3, a plot of the data obtained from static light-scattering measurements is shown in Figure 3 (the bottom line). From the slope the standard enthalpy of micellization at temperatures between 48 and 55 °C was found to be −240 ± 10 kJ mol^{-1}. The other standard thermodynamic quantities at 50 °C were $\Delta G° = -33$ kJ mol^{-1} and $T\Delta S° = -207$ kJ mol^{-1}. These values clearly indicate that the micellization of the copolymer concerned is an enthalpy-driven process. The large negative standard enthalpy of micellization, arising from the extensive attractive interactions between the insoluble block segments, outweighs the opposing entropic factors which tend to disperse the polymer chains randomly throughout the solution. For polystyrene-*b*-polyisoprene copolymers in *n*-hexadecane, Price et al.[18] reported that $\Delta G°$ and $\Delta H°$ values became more negative when the length of the core-forming block was increased. Very interestingly, the enthalpy results for block copolymers in organic selective solvents are in strong contrast with those obtained for aqueous solutions of water-soluble copolymers. For example, a strongly positive $\Delta H°$ value of about 200–400 kJ mol^{-1} was obtained for an aqueous solution of poly(oxyethylene)–poly(oxypropylene)–poly(oxyethylene) copolymers,[11,12] whereas $\Delta G°$ remained ~20 kJ mol^{-1}. It is likely that, in this case, hydrophobic interactions of entropy origin, although considerably weaker than in the case of low molecular weight surfactants in water, are mainly responsible for micelle formation, implying that the micellization process is entropy driven due to the structural change in water on removal of the hydrocarbon-like units.

3. Static and Dynamic Properties in Three Regions. Static and dynamic properties of the copolymer solution were examined in detail at three temperatures: 25, 45, and 60 °C. For micellar solutions the Debye equation is applicable in the dilute solution regime,

$$K(C - \text{cmc})/R_{vv,\theta} = 1/M_w + 2A_2(C - \text{cmc}) \quad (4)$$

where K ($=4\pi^2 n_0^2 (\text{d}n/\text{d}C)^2/N_A\lambda_0^4$) is an optical constant with N_A, n_0, and λ_0 being Avogadro's number, the refractive index of the solvent, and the wavelength of light in vacuo. $R_{vv,\theta}$ is the excess Rayleigh ratio at a scattering angle θ with vertically polarized incident and scattered beams, C is the total concentration in grams per milliliter, and A_2 is the second virial coefficient. For all the solutions examined at 60 °C, the forward scattering and the backward scattering were the same, whereas at 25 and 45 °C a remarkable angular dependence of scattered intensity was observed. In the latter case, the R_{vv} values extrapolated to zero scattering angle were used in putting eq 4 to use (Figure 4b and the bottom line in Figure 4a). Also,

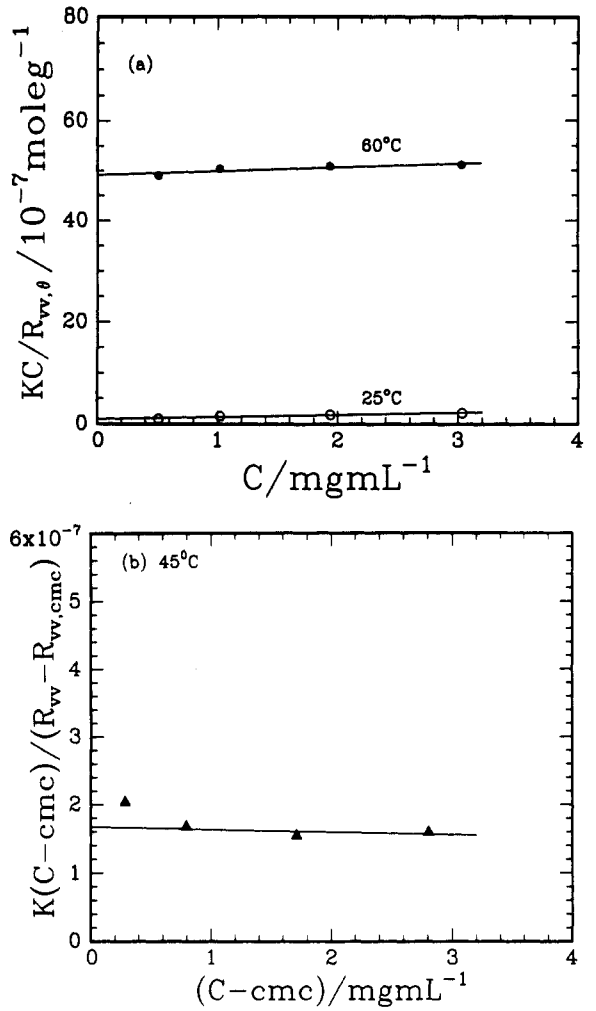

Figure 4. (a) Plots of $KC/R_{vv,\theta}$ versus concentration for the PS-*b*-P(*t*-BS) copolymer in DMA at 25 and 60 °C. (b) Plot of $K(C - cmc)/(R_{vv} - R_{vv,cmc})$ versus $(C - cmc)$ for the same system at 45 °C. The data at 25 and 45 °C are the values extrapolated to zero scattering angle.

Table I
Refractive Index Increment of Block Copolymer in DMA[a]

temp (°C)	$(dn/dC)_{PS}$[b] (cm^3 g^{-1})	$(dn/dC)_{P(t\text{-}BS)}$[c] (cm^3 g^{-1})	dn/dC[d] (cm^3 g^{-1})
25.0	0.166	0.124	0.141
45.0	0.168	0.127	0.143
60.0	0.170	0.129	0.145

[a] The dn/dC value of the homopolymer in DMA was calculated by using the Gladstone and Dale formula.[22] [b] At 25 °C $n_{PS} = 1.61$ and $d_{PS} = 1.05$ g mL^{-1} were taken. [c] At 25 °C $n_{P(t\text{-}BS)} = 1.563$ and $d_{P(t\text{-}BS)} = 1.026$ g mL^{-1} were taken. [d] Calculated by eq 5 in the text.

additional information on the radius of gyration ($\langle R_g^2\rangle_{z,app}$, apparent *z*-averaged squared radius of gyration for the block copolymer) can be obtained from the limiting slope of the $[K(C - cmc)/R_{vv}]_{c=0}$ versus q^2 plot with q $(=(4\pi/\lambda)\sin(\theta/2))$ being the scattering vector.

The refractive index increment of the copolymer solution can be calculated using the relation

$$dn/dC = w_A(dn/dC)_A + w_B(dn/dC)_B \quad (5)$$

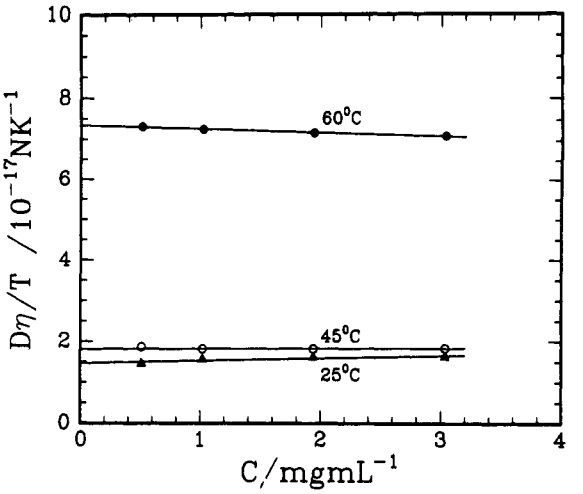

Figure 5. Plots of the reduced diffusion coefficient $D\eta/T$ versus concentration for the PS-*b*-P(*t*-BS) copolymer in DMA at different temperatures.

where w is the weight fraction and the subscripts A and B denote the component blocks, PS and P(*t*-BS), respectively. All the dn/dC values estimated for the copolymer and the two homopolymers are given in Table I. For block copolymers which are usually heterogeneous in chemical composition, eq 4 yields an apparent molecular weight ($M_{w,app}$) rather than a true weight-average molecular weight (M_w). A correction can be made by using the relation[19]

$$M_{w,app}(dn/dC)^2 = M_w(dn/dC)_A(dn/dC)_B + [(dn/dC)^2_A - (dn/dC)_A(dn/dC)_B]w_AM_w^A + [(dn/dC)^2_B - (dn/dC)_A(dn/dC)_B]w_BM_w^B \quad (6)$$

where M_w^A and M_w^B are the weight-average molecular weights of the components. In our case, as shown in Table II, the correction by eq 6 led to a maximum variation of ~3%.

Figure 4 shows the Debye plots in the concentration range 0.51–3.04 mg mL^{-1}. It should be noted that at 60 °C only unimers are present; therefore the total concentration can simply be used. At 25 °C the cmc term can be neglected because of its very small value (likely, $\sim 5 \times 10^{-4}$ mg mL^{-1}). In contrast, at 45 °C the cmc term (~0.23 mg mL^{-1}) must be included (Figure 4b). Thus, the weight-average molecular weight M_w, the aggregation number n_w, and the second virial coefficient A_2, together with the $\langle R_g^2\rangle^{1/2}_{z,app}$ data, are listed in Table II. Importantly, the M_w values of 2.0×10^5 g mol^{-1} at 60 °C ($n_w = 1$) and 1.0×10^7 g mol^{-1} at 25 °C ($n_w = 54$) provide experimental proof that when the temperature is varied, the unimer and micelle exist at the two extreme regions, respectively. Although there are some uncertainties associated with the estimated dn/dC values in Table I, it does not prevent us from drawing this conclusion.

We have also examined the dynamic properties for the copolymer solution. It should be noted that for the data analysis of the present micellar system, the internal motion contributions, if any, can be neglected since $qR_g < 1$. The corresponding concentration dependence plots based on the cumulants analysis are given in Figure 5, where the

Table II
Static and Dynamic Properties of PS-*b*-P(*t*-BS) in DMA

temp (°C)	$M_{w,app}$ (g mol^{-1})	M_w (g mol^{-1})	A_2 (cm^3 mol g^{-2})	n_w	D_0 (cm^2 s^{-1})	R_h (nm)	$\langle R_g^2\rangle^{1/2}_{z,app}$ (nm)
25.0	1.03×10^7	9.96×10^6	2.0×10^{-5}	54	4.71×10^{-8}	50.0	31.5
45.0	5.99×10^6	5.75×10^6	-1.9×10^{-6}	31	7.97×10^{-8}	40.5	26.8
60.0	2.03×10^5	2.05×10^5	3.7×10^{-5}	1	4.01×10^{-7}	10.0	

reduced diffusion coefficient ($=D\eta/T$) is employed to allow for the effects of temperature and viscosity in the Einstein–Stokes equation,

$$D = kT/(6\pi\eta R_h) \quad (7)$$

In so doing, the reciprocal intercept in Figure 5 is a measure of the particle size of interest. The D_0 (diffusion coefficient at infinite dilution) and R_h values derived are listed in Table II. As seen from Figure 5, there is a large difference in R_h between, on the one side, 25 and 45 °C, and on the other side, 60 °C, which is entirely in accordance with the molecular weight data.

The solution behavior at 45 °C is of interest. For the most dilute solution used in this work ($C = 0.51$ mg mL^{-1}), as analyzed below, an appreciable amount of unimers coexisting with micelles was found, the scattered intensity ratio of unimer to micellar particle being ~1:40 and the corresponding weight ratio ~0.78:1. However, at higher concentrations the micelles became the predominant form in the system and the KC/R_{vv} values (extrapolated to zero scattering angle and corrected for the cmc) were nearly constant, as shown in Figure 4b. Thus, a linear extrapolation in Figure 4b yields a M_w value of 5.75×10^6 g mol^{-1} for the micelle species at 45 °C.

Assuming that the micellar particles formed at 25 and 45 °C are spherical in shape, we would have the relation $M \propto R^3$. Such a scaling behavior is approximately observed when we compare the M_w and R_h data at 25 and 45 °C (see Table II). Furthermore, it is known that the ratio of radius of gyration to hydrodynamic radius for a given system serves to distinguish between different structures.[20] For example, a value of 0.77 is predicted for the hard-sphere model and the ratio is equal to or larger than unity for other structures. The R_g and R_h data listed in Table II give a value of 0.63–0.68 for their ratio. Based on the above arguments and keeping in mind that the R_g measured for the block copolymer is an apparent value, it is acceptable that the copolymer micelles studied can be viewed as spheres consisting of a compact P(t-BS) core surrounded by a swollen PS shell.

Very recently, Phoon et al.[21] studied the dilute solutions of PS-b-P(t-BS) in dimethylformamide (DMF) at 20 °C and reported that the micelles formed have a molecular weight of 5.3×10^7 g mol^{-1} and a R_h of 66 nm. Although there is some difference between DMA and DMF, we could expect that in either DMA or DMF, in the micelle region the copolymer micelles become increasingly large with decreasing temperature until the phase separation temperature is reached.

4. Equilibrium between Unimers and Micelles in the Transition Region. Parts a and b of Figure 6 show the logarithmic unnormalized first-order electric field correlation function $\beta^{1/2}g^{(1)}(\tau)$ as a function of delay time τ at different temperatures for the 0.51 and 3.04 mg mL^{-1} solutions, respectively. Here β is a constant depending on the scattering geometry and is usually determined by a fit to the experimental data. In order to directly compare the relaxation behavior at different temperatures, the physical quantity reduced delay time ($=\tau T/\eta$) is used. For the 0.51 mg mL^{-1} solution, as clearly seen from Figure 6a, the top curve (25 °C) as well as the two bottom curves (55 and 60 °C, essentially identical) exhibits a single-exponential decay character but with largely differing relaxation rates. Correspondingly, from the slope, monodisperse particle radius values of 50.3 (25 °C) and 9.8 nm (55 and 60 °C) are obtained. As far as the intermediate temperature region (45–50 °C) is concerned, all the correlation function curves consistently reveal a multiexponential

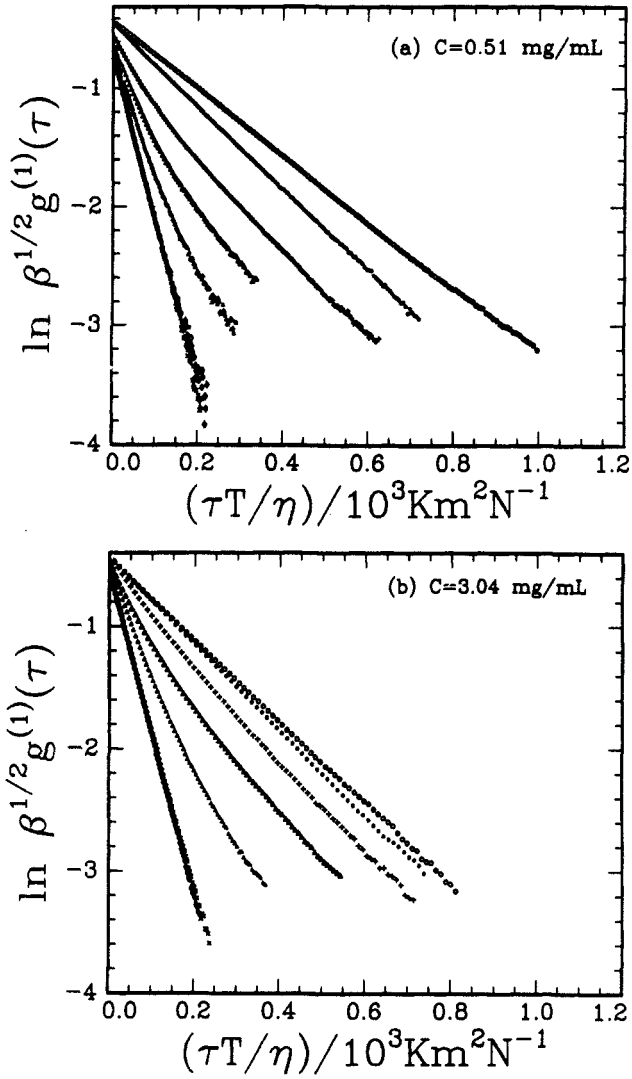

Figure 6. Plots of the logarithmic electric field correlation function against reduced delay time. (a) $C = 0.51$ mg mL^{-1}. From top to bottom the temperatures are 25, 45, 48, 49, 50, 55 (crosses), and 60 °C (diamonds) respectively. (b) $C = 3.04$ mg mL^{-1}. From top to bottom the temperatures are 25, 45, 53, 54, 55, 60 (crosses), and 65 °C (diamonds), respectively.

nature, the curve location and shape being strongly temperature-dependent. Regarding the relaxation rate, all the intermediate curves are constrained within the frame defined by the top and bottom curves. Obviously, in this region a dynamic equilibrium, which shifts toward micelles with decreasing temperature, is established between single copolymer chains and polymolecular micelles. As shown in Figure 6b, the relaxation behavior at higher concentration ($C = 3.04$ mg mL^{-1}) is very similar to that displayed in Figure 6a. The difference is that the temperature scale is now shifted toward higher temperature. For instance, on the low-temperature side, the single-exponential decay associated with the formation of nearly monodisperse micelles has been extended to 45 °C. Similarly, on the high-temperature side, the fast single-exponential decay first appeared at 55 °C instead of 50 °C. This means that the equilibrium is not only temperature-dependent but also concentration-dependent.

As mentioned above, for the unimer and micelle species the characteristic relaxation rates are well separated (a factor of 4–5), and both species are narrow in their size distribution. Therefore it seems possible, by the use of the CONTIN analysis, to obtain some quantitative insights into the equilibrium between unimers and micelles in the

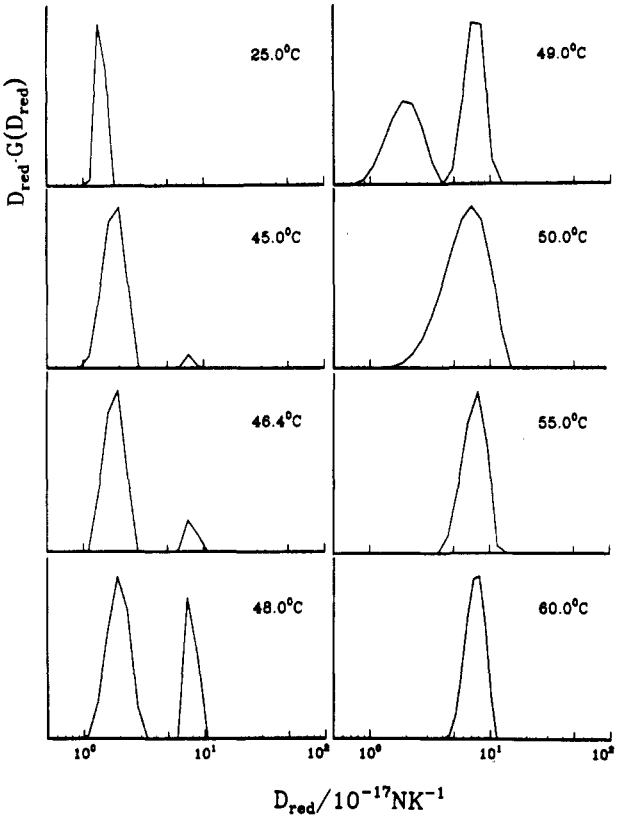

Figure 7. Relaxation rate distributions at the indicated temperatures obtained by the CONTIN analysis of the field correlation function of the 0.51 mg mL^{-1} copolymer solution. The reduced diffusion coefficient ($D\eta/T$) was used to compare directly the peak locations at different temperatures. The peak area represents the scattered intensity contribution.

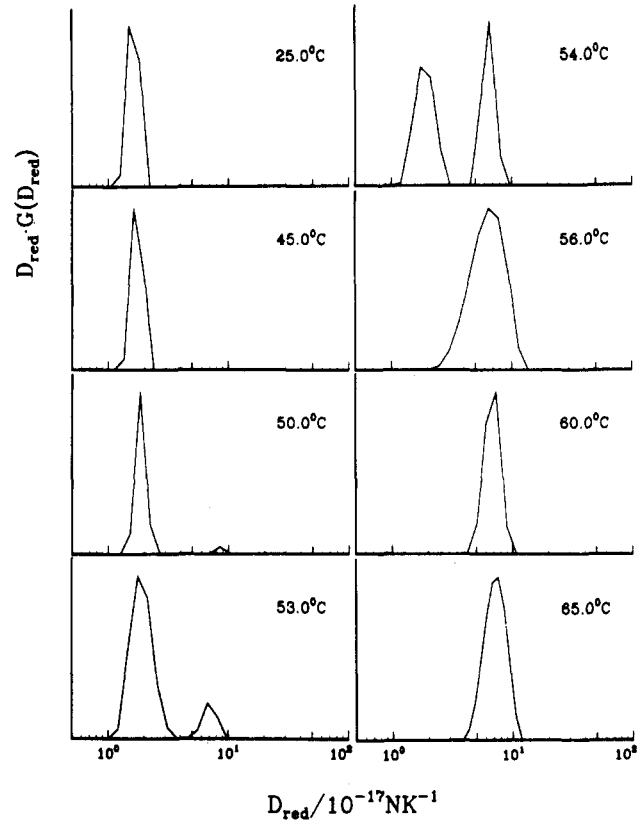

Figure 8. Relaxation rate distributions at the indicated temperatures for the 3.04 mg mL^{-1} copolymer solution.

transition region. For a polydisperse system,

$$g^{(1)}(\tau) = \int_0^\infty G(\Gamma) \exp(-\Gamma\tau)\, d\Gamma \quad (8)$$

or

$$g^{(1)}(\tau) = \int_0^\infty \Gamma G(\Gamma) \exp(-\Gamma\tau)\, d \ln \Gamma \quad (9)$$

with $\Gamma = Dq^2$ where $G(\Gamma)$ is the characteristic linewidth (or relaxation rate) distribution function with Γ being the linewidth or relaxation rate. The mean characteristic linewidth $\bar{\Gamma}$, the second moment μ_2, and the variance are defined by

$$\bar{\Gamma} = \int G(\Gamma)\, d\Gamma$$

$$\mu_2 = \int G(\Gamma)\, (\Gamma - \bar{\Gamma})^2\, d\Gamma$$

$$\text{Var} = \mu_2/\bar{\Gamma}^2$$

The CONTIN method, as a constrained regularization technique developed by Provencher,[15] nowadays becomes a routine approach to extract $G(\Gamma)$ from the measured $g^{(1)}(\tau)$. Note that because of the ill-posed nature of the Laplace inversion of eq 8, CONTIN gives the most probable solution among a number of fitted solutions.

Figures 7 and 8 show the results obtained by the CONTIN method for the 0.51 and 3.04 mg mL^{-1} copolymer solutions, respectively. The relaxation rate distributions in terms of the reduced diffusion coefficient $D_{red}(=D\eta/T$, note that $\Gamma \propto D_{red}$) are conveniently given in the semilogarithmic form, i.e., $D_{red}G(D_{red})$ versus log D_{red}. The advantages of such plot are (1) peak locations can be compared directly for different temperatures, (2) the area is a direct measure of the scattering intensity contribution, and (3) there is no assumption made about the geometrical shape of single copolymer chains. $D_{red}G(D_{red})$ is expressed in arbitrary units but normalized to the highest value at each temperature to facilitate comparisons.

As shown in Figure 7, the relaxation rate distributions at the two extreme temperatures studied reveal a narrow peak in each case, as predicted: a fast unimer peak at 60 °C and a slow micelle peak at 25 °C. Upon cooling down from 60 °C, the distribution function first becomes broader at 50 °C but still keeps the unimodal nature, meaning that only a small amount of micelles is formed. Correspondingly, an increase of ~21% in the scattered intensity as compared to that at 60 °C is seen in Figure 1. A bimodal distribution has been initiated at 49 °C with an intensity ratio of micelle to unimer (I_m/I_u) of 0.83/1. A further small reduction in temperature (only a few centigrade degrees) leads to a remarkably increasing contribution of micelles to the scattered intensity (I_m/I_u are 2.3/1 and 9.4/1 at 48 and 46.4 °C, respectively). As can be seen from Figure 7, at 45 °C the micelle contributes a major part of the scattered intensity, the I_m/I_u ratio being about 40/1. A unimodal relaxation rate distribution associated with the micelle species appears upon a further decrease in temperature. Therefore, the CONTIN analysis of the measured autocorrelation function as a function of temperature gives, in a more or less quantitative manner, a clear picture about the temperature-dependent dynamic equilibrium between single polymer chains and associated structures. Figure 8 illustrates the similar properties in the relaxation rate distribution for the 3.04 mg mL^{-1} solution. A comparison between Figures 7 and 8 has led to an important conclusion that the upper and lower boundaries of the temperature region where the bimodal distribution exists shift to higher temperature with increasing concentration.

We may go further in using the CONTIN results. According to the mass action law model of micelle

Table III
Critical Micelle Concentration and Standard Thermodynamic Functions of Micellization

	cmc (mg/mL)		$\Delta G°$ (kJ/mol)		$\Delta H°$ (kJ/mol)	
temp (°C)	IF method[a]	CONTIN	IF method	CONTIN	IF method	CONTIN
45.0	0.23	0.25	-36	-36		
46.4	0.34	0.46	-35	-34		
48.0	0.53	0.58	-34	-34	-240 (48–55 °C)	-270 (45–54 °C)
49.0	0.70	0.63	-33	-33		
50.0	0.93	1.8	-33	-31		
53.0	2.1	2.9	-31	-30		
54.0	2.8	3.6	-30	-29		

[a] Based on the scattered intensity inflection as shown in Figure 1.

formation we may assume that a *single* micellar species with an aggregation number n is in equilibrium with the unimers:

$$nA_1 \rightleftharpoons A_n \tag{10}$$

Therefore[17]

$$K_{eq} = [A_n]/[A_1]^n \tag{11}$$

and

$$\text{cmc} \simeq K_{eq}^{(-1/(n-1))} \tag{12}$$

where $[A_1]$ and $[A_n]$ are the molar concentrations of unimer and micelle (n-mer), respectively. As described above, the relative intensity contributions made by unimers and micelles in the mixture can be obtained using the CONTIN analysis. Assuming that the solution is thermodynamically ideal and the refractive index increment is approximately the same for both unimer and micelle species, the ratio I_m/I_u can be further related to the concentration and molecular weight of each species by the expression

$$I_m/I_u \simeq (C_m M_m)/(C_u M_u) \tag{13}$$

where C_m and C_u are in grams per milliliter. As shown in Figure 7, I_m/I_u values of 40/1, 9.4/1, 2.3/1, and 0.83/1 were obtained for the 0.51 mg mL^{-1} solution at 45, 46.4, 48, and 49 °C, respectively. By combination of eqs 11 and 12 with eq 13, an attempt has been made by us to calculate the cmc value through K_{eq} derived from the CONTIN results.

Knowing M_m at 45 °C (see Table II) and M_u (=1.85 × 10^5 g mol^{-1}) and assuming that in the transition region the M_w value is approximately constant over a relatively narrow temperature range, we obtained weight fraction values of 0.56, 0.23, 0.069, and 0.026 for micelles (in equilibrium with unimers) from the above CONTIN results. The calculated cmc values together with those obtained on the basis of the data given in Figure 3 (the bottom line), are listed in Table III. As shown in Figure 8, the I_m/I_u values for the 3.04 mg mL^{-1} solution are 27/1, 7.1/1, and 1.2/1 at 50, 53, and 54 °C, respectively. Then, the cmc value could also be estimated by the same procedure for these three temperatures. Moreover, standard free energy and standard enthalpy of micellization were calculated and are listed in Table III. As seen from Table III, in general, the agreement between the two sets of results, obtained by two different approaches, seems quite good, if we consider that several assumptions to simplify the treatment have been made. In particular, the real unimers and micelles have never been strictly monodisperse and the uncertainties associated with the CONTIN analysis for a broadly polydisperse system are not trivial. Importantly, for the dilute solution (C = 0.51 mg mL^{-1}) the cmc values calculated from the CONTIN results are very close to those experimentally determined by using the inflection point on the scattered intensity curve, the difference in most cases being only 10%. At higher concentration (C = 3.04 mg mL^{-1}) relatively large differences of about 30–100% in the cmc values were observed as expected, since in this case the assumption on the ideality of solution may not be valid. This nonideality behavior for the micelles is implicated in Figure 2 where the two R_h lines cross for the micelles at two different concentrations. For the standard thermodynamic functions, the agreement between the two methods is satisfactory in all cases.

The intensity data given in Figure 1 can also be used to estimate the weight fraction of unimers and micelles in the transition region and therefore to determine the equilibrium constant or the cmc value. For a mixture in equilibrium the measured scattered intensity is the sum of the contributions made by unimers and micelles,

$$I = I_u^0 C_u + I_m^0 C_m \tag{14}$$

where I_u^0 and I_m^0 are the scattered intensity of the unimer and micelle species in ideally dilute solution at unit weight concentration, respectively. In our case, the I_u^0 value is known from the intensity data in the unimer region and I_m^0 can be estimated by the relation $I_m^0 = I_u^0 M_m/M_u$, since both M_m (at 45 °C) and M_u are known. Here we have again implicitly assumed that the M_m value is approximately constant in the transition region. Thus, when the total scattered intensity of the solution at a given concentration is known, the weight concentration of each component can be calculated. When this approach was followed, for example, weight fraction values of 0.55, 0.25, 6.2 × 10^{-2}, and 2.7 × 10^{-2} were obtained for micelles in the 0.51 mg mL^{-1} solution at 45, 46.4, 48, and 49 °C, respectively, which are in good agreement with those derived from the CONTIN results. Furthermore, on the basis of the mass action law the cmc values were also calculated. All the results together with those obtained by the CONTIN approach are summarized in Figure 3 (the top line). A least squares fit yields a ΔH^0 value of −270 ± 10 kJ mol^{-1}, which agrees with that obtained by monitoring the temperature dependence of scattered intensity.

In summary, the internal consistency between the results of two different approaches, i.e., the time-averaged scattered intensity measurement and the intensity fluctuation measurement, is of importance, indicating that although some assumptions are made to reduce the data analysis, a quantitative (or semiquantitative) understanding of the association behavior for the present system can be achieved by using the light-scattering technique.

Conclusions

In contrast to the PEO–PPO–PEO/water system for which an increase in temperature leads to remarkable micelle formation (an entropy-driven process), the micellization of PS-*b*-P(*t*-BS) in a polar solvent, *N*,*N*-

dimethylacetamide, takes place by decreasing the temperature (an enthalpy-driven process). Both of them exhibit three temperature regions (unimer, transition, and micelle regions) by changing the temperature, but in opposite directions. For the present system, the transition region where micelles are in equilibrium with single polymer chains is reasonably sharp because of (1) the narrow size polydispersity of both the unimers and the micellar particles formed, (2) the better composition homogeneity of the block copolymer studied as compared to the commercial poloxamer copolymer used in a previous study,[6] and (3) the strong temperature dependence of the solvent quality of DMA with respect to the P(*t*-BS) block. These features enable us to use the CONTIN analysis as well as the intensity analysis to extract valuable quantitative information on the temperature-dependent equilibrium between unimers and associated structures, including the estimation of the critical micelle concentration and related thermodynamic properties.

Acknowledgment. We gratefully acknowledge support of this research by the National Science Foundation, Division of Materials Research, Polymers Program (DMR 8921968), the U.S. Department of Energy (DEFG0286-ER45237), and the U.S. Army Research Office (DAAL0391-G0040).

References and Notes

(1) Tuzar, Z.; Kratochvil, P. *Adv. Colloid Interface Sci.* **1976**, *6*, 201.
(2) Price, C. *Pure Appl. Chem.* **1983**, *55*, 1563.
(3) Brown, R. A.; Masters, A. J.; Price, C.; Yuan, X. F. In *Comprehensive Polymer Science*; Booth, C., Price, C., Eds.; Pergamon Press: Oxford, U.K., 1989; Vol. 2, Chapter 6.
(4) Zhou, Z.; Chu, B. *Macromolecules* **1987**, *20*, 3089.
(5) Zhou, Z.; Chu, B. *Macromolecules* **1988**, *21*, 2548.
(6) Zhou, Z.; Chu, B. *J. Colloid Interface Sci.* **1988**, *126*, 171.
(7) Wanka, G.; Hoffmann, H.; Ulbricht, W. *Colloid Polym. Sci.* **1990**, *268*, 101.
(8) Brown, W.; Schillen, K.; Almgren, M.; Hvidt, S.; Bahadur, P. *J. Phys. Chem.* **1991**, *95*, 1850.
(9) Wu, G.; Zhou, Z.; Chu, B. *Macromolecules*, accepted for publication.
(10) (a) Plestil, J.; Hlatava, D.; Hrouz, J.; Tuzar, Z. *Polymer* **1990**, *31*, 2112. (b) Tuzar, Z.; Konak, C.; Stepanek, P.; Plestil, J.; Kratochvil, P.; Prochazka, K. *Polymer* **1990**, *31*, 2118.
(11) Reddy, N. K.; Fordman, P. J.; Attwood, D.; Booth, C. *J. Chem. Soc., Faraday Trans.* **1990**, *86*, 1569.
(12) Deng, Y.; Yu, G.-E.; Price, C.; Booth, C. *J. Chem. Soc., Faraday Trans.* **1992**, *88*, 1441.
(13) Quintana, J. R.; Villacampa, M.; Munoz, M.; Andrio, A.; Katime, I. A. *Macromolecules* **1992**, *25*, 3125, 3129.
(14) Quintana, J. R.; Villacampa, M.; Salazar, R.; Katime, I. A. *J. Chem. Soc., Faraday Trans.* **1992**, *88*, 2739.
(15) (a) Provencher, S. W. *Makromol. Chem.* **1979**, *180*, 201. (b) Provencher, S. W. *Comput. Phys. Commun.* **1982**, *27*, 213, 229.
(16) Koppel, D. E. *J. Chem. Phys.* **1972**, *57*, 4814.
(17) Lindman, B.; Wennerstrom, H. *Top. Curr. Chem.* **1980**, *87*, 1.
(18) Price, C.; Chan, E. K. M.; Stubbersfield, R. B. *Eur. Polym. J.* **1987**, *23*, 649.
(19) Benoit, H.; Froelich, D. In *Light Scattering from Polymer Solutions*; Huglin, M., Ed.; Academic Press: London, 1972.
(20) Burchard, W. *Adv. Polym. Sci.* **1983**, *48*, 1.
(21) Phoon, C. L.; Higgins, J. S.; Burchard, W.; Peiffer, D. G. *Macromol. Rep.* **1992**, *A29* (Suppl. 2), 179.
(22) Outer, P.; Carr, C. I.; Zimm, B. H. *J. Chem. Phys.* **1950**, *18*, 830.